


From UV to Near-Infrared Light-Responsive Metal–Organic Framework Composites: Plasmon and Upconversion Enhanced Photocatalysis

Dandan Li, Shu-Hong Yu, and Hai-Long Jiang*

The exploitation of photocatalysts that harvest solar spectrum as broad as possible remains a high-priority target yet grand challenge. In this work, for the first time, metal–organic framework (MOF) composites are rationally fabricated to achieve broadband spectral response from UV to near-infrared (NIR) region. In the core–shell structured upconversion nanoparticles (UCNPs)-Pt@MOF/Au composites, the MOF is responsive to UV and a bit visible light, the plasmonic Au nanoparticles (NPs) accept visible light, whereas the UCNPs absorb NIR light to emit UV and visible light that are harvested by the MOF and Au once again. Moreover, the MOF not only facilitates the generation of “bare and clean” Au NPs on its surface and realizes the spatial separation for the Au and Pt NPs, but also provides necessary access for catalytic substrates/products to Pt active sites. As a result, the optimized composite exhibits excellent photocatalytic hydrogen production activity ($280 \mu\text{mol g}^{-1} \text{h}^{-1}$) under simulated solar light, and the involved mechanism of photocatalytic H_2 production under UV, visible, and NIR irradiation is elucidated. Reportedly, this is an extremely rare study on photocatalytic H_2 production by light harvesting in all UV, visible, and NIR regions.

Evoked by the present energy and environmental issues, efficient utilization of renewable energy is in high demand. As one of the most promising renewable energy sources, solar energy offers a free, clean, and infinite resource. Photocatalysis, converting solar energy to chemical energy, holds great promise to address the current and future demand of energy supply.^[1] Solar spectrum is constituted by 5% UV, 42–45% visible, and more than 50% near-infrared (NIR) light. The currently most studied photocatalysts, semiconductors, and related materials, mostly absorb UV light only, and some of them are responsive to visible light more or less, limiting solar energy utilization.

Dr. D. Li, Prof. S.-H. Yu, Prof. H.-L. Jiang
Hefei National Laboratory for Physical Sciences at the Microscale
CAS Key Laboratory of Soft Matter Chemistry
Collaborative Innovation Center of Suzhou Nano Science and Technology
Department of Chemistry
University of Science and Technology of China
Hefei, Anhui 230026, P. R. China
E-mail: jianglab@ustc.edu.cn

 The ORCID identification number(s) for the author(s) of this article can be found under <https://doi.org/10.1002/adma.201707377>.

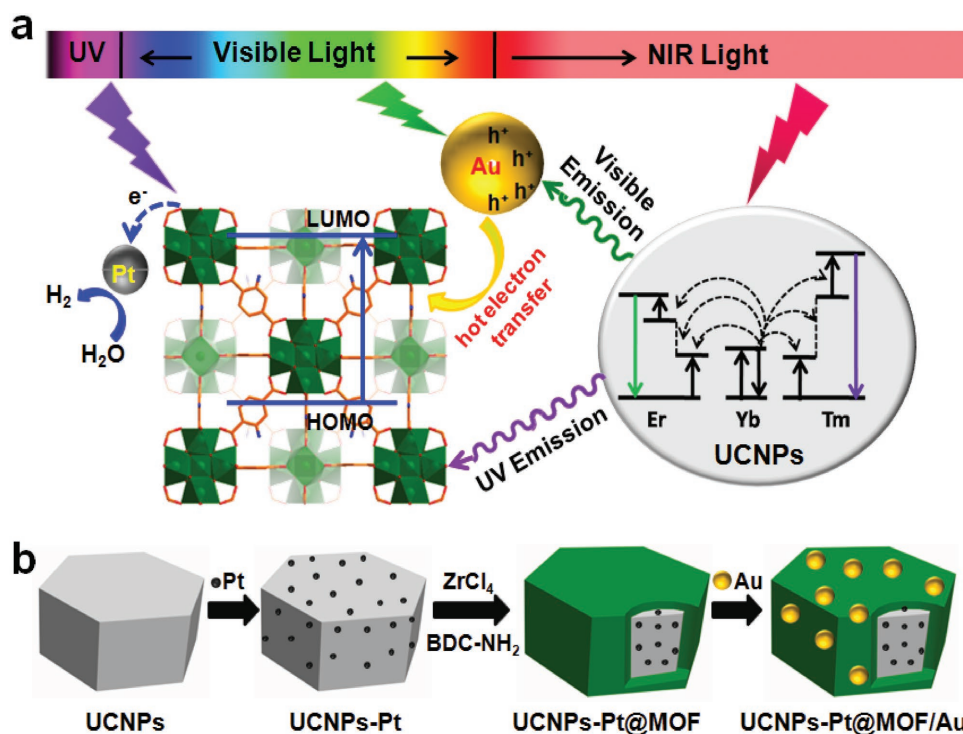
DOI: 10.1002/adma.201707377

To date, very limited NIR-responsive photocatalysts have been developed.^[2] Particularly, the search for photocatalysts, which harvest solar spectrum from UV to NIR region, to achieve high solar energy utilization is a highly desired target.

To meet this grand challenge, various strategies have been developed to extend the light response of photocatalysts from UV to visible region.^[3,4] Amongst them, the hybridization with plasmonic metal nanostructures was recognized to be one of the most promising approach, as plasmonic metals possessing surface plasmon resonance (SPR) effect induce strong absorption in visible region, breaking through the UV-responsive limit of many photocatalysts.^[4] It has been well demonstrated that Au NPs with a clean surface merit their direct contact with other components and thus improve photocatalytic efficiency.^[4e] Nevertheless, the use of NIR light for photocatalysis remains very rare, possibly due to its low photon energy and

no response to NIR light of common catalysts. In this context, lanthanide-doped upconversion nanoparticles (UCNPs) are able to convert longer wavelength irradiation (e.g., NIR) to shorter wavelength emission (e.g., UV and/or visible),^[5] which can be then re-absorbed by adjacent UV/vis-responsive components. Therefore, the rational integration of lanthanide-doped UCNPs and UV/vis-responsive components gives rise to composite materials, in which the exertion of their respective functions would make full solar light harvesting possible for photocatalysis.

Bearing the above points in mind, metal–organic frameworks (MOFs), a class of crystalline porous materials featuring diversified and tailorable structures,^[6,7] would be judicious candidates. In this work, for the first time, novel broadband spectrum-responsive MOF composites with a core–shell architecture, UCNPs-Pt@MOF/Au (UCNPs denote $\text{NaYF}_4\text{:Yb, Tm, Er}$), which capture UV, visible, and NIR photons based on both plasmon and upconversion, have been fabricated for photocatalytic H_2 production. The MOF is mostly responsive to UV light, the plasmonic Au absorbs visible light, while the UCNPs upconvert NIR light to UV and visible light, which are harvested by the MOF and Au once again, giving rise to light harvesting from UV to NIR region (Scheme 1a). Moreover, the MOF realizes the spatial separation for Au and Pt NPs, enables catalytic



Scheme 1. a) The light absorption of each component in the MOF composites and involved mechanism for photocatalytic hydrogen production. b) Schematic illustration of synthetic process for the UCNPs-Pt@MOF/Au composites.

substrates/products accessible to Pt active sites, and also facilitates the generation of “bare and clean” Au NPs (Scheme 1b). In addition, the MOF shell can be facily grown on the UCNPs with controllable thickness by a layer-by-layer assembly method. Remarkably, the optimized UCNPs-Pt@MOF/Au composite exhibits excellent H₂ production rate by adjusting the thickness of MOF-shell and Au content, under simulated solar light irradiation. To our knowledge, this is an extremely rare report on a catalyst harnessing light falling in all UV, visible, and NIR regions for photocatalytic H₂ production.^[2e]

The representative MOF, UiO-66-NH₂ (Zr₆O₄(OH)₄(BDC-NH₂)₆, BDC-NH₂ = 2-amino-1,4-benzenedicarboxylic acid),^[6e] was employed to fabricate the composites. UiO-66-NH₂ features a 3D network involving tetrahedral and octahedral cages of 6 and 11 Å, respectively, accessible through microporous openings (4–6 Å), very high stability, as well as high surface area, suitable for stabilizing metal NPs and mass transport. The core-shell structured MOF composites, denoted UCNPs-Pt@MOF/Au, were synthesized by a stepwise approach (Scheme 1b). In the first step, a hydrothermal method was employed to synthesize UCNPs with a platelike morphology. The Pt NPs were deposited onto the surface of UCNPs decorated with polyvinyl pyrrolidone (PVP) layer, followed by alternately anchoring Zr(IV) and BDC-NH₂ linker for continuous growth of the MOF shell, and finally “bare and clean” Au NPs were stabilized on the MOF to afford the composites (Section S2, Supporting Information), in which the MOF thickness (Section S3, Supporting Information) and Au loading amount were controllable. The MOF shell is subjected to six cycles of growth to give UCNPs-Pt@MOF, and the optimized 0.3 wt% Au loading in UCNPs-Pt@MOF/Au, which are default hereafter unless otherwise stated.

The UCNPs nanoplates are in ≈450 nm sizes (Figure 1a), and ≈3 nm Pt NPs are well-dispersed on their external surfaces (Figure 1b; Figure S1, Supporting Information). Upon MOF layer growth, the clear-cut contrast between MOF and UCNPs-Pt evidently suggest the formation of a core-shell architecture with the thickness of MOF shell of ≈40 nm (Figure 1c). It is worth noting that the MOF shell thickness can be facily regulated by alternated addition of ZrCl₄ and BDC-NH₂ (Figure S2, Supporting Information). The MOF shell with a high surface area would facilitate the transport of reactants and subsequent catalysis (Figure S3, Supporting Information). Similarly, the Au content is readily modulated by controlling HAuCl₄ solution volume. The isolated Au NPs in the range of 9–12 nm evenly distribute on the surface of UCNPs-Pt@MOF particles (Figure 1d; Figure S4, Supporting Information), leading to the final UCNPs-Pt@MOF/Au composites. Infrared (IR) spectra support the successful formation of UiO-66-NH₂ (Figure 2a). The typical stretching modes of –NH₂ located at 3460 and 3370 cm⁻¹ are observable for UCNPs-Pt@MOF/Au composite, along with the vibration peak at 772 and 652 cm⁻¹, which are characteristic absorption peaks of the benzene unit. Powder X-ray diffraction (PXRD) pattern for UCNPs-Pt@MOF/Au further verifies this point, though the main peaks at 7°–10° are weak due to the low-content and thin MOF shell (Figure 2b).

The UV–vis–NIR absorption spectrum of UCNPs displays significant change after subsequent MOF growth (Figure 2c). Both UCNPs and UCNPs-Pt exhibit a main absorption band at 980 nm, corresponding to the transition of Yb³⁺.^[5a] Upon coating with UiO-66-NH₂, a strong absorption mainly located at ≈300–450 nm (UV region) arises due to the MOF absorption. When Au NPs are deposited, an obvious

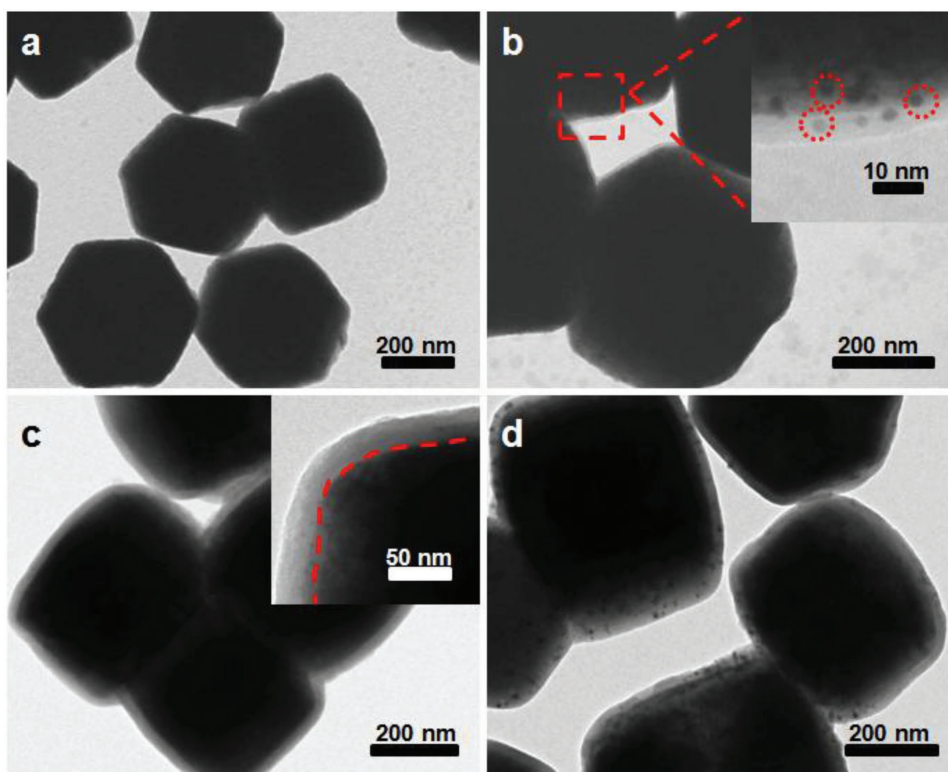


Figure 1. TEM images of (a) UCNPs, (b) UCNPs-Pt (insert: Pt NPs deposited on the surface of UCNPs), (c) UCNPs-Pt@MOF (insert: the clear-cut contrast between the MOF and UCNPs), and (d) UCNPs-Pt@MOF/Au.

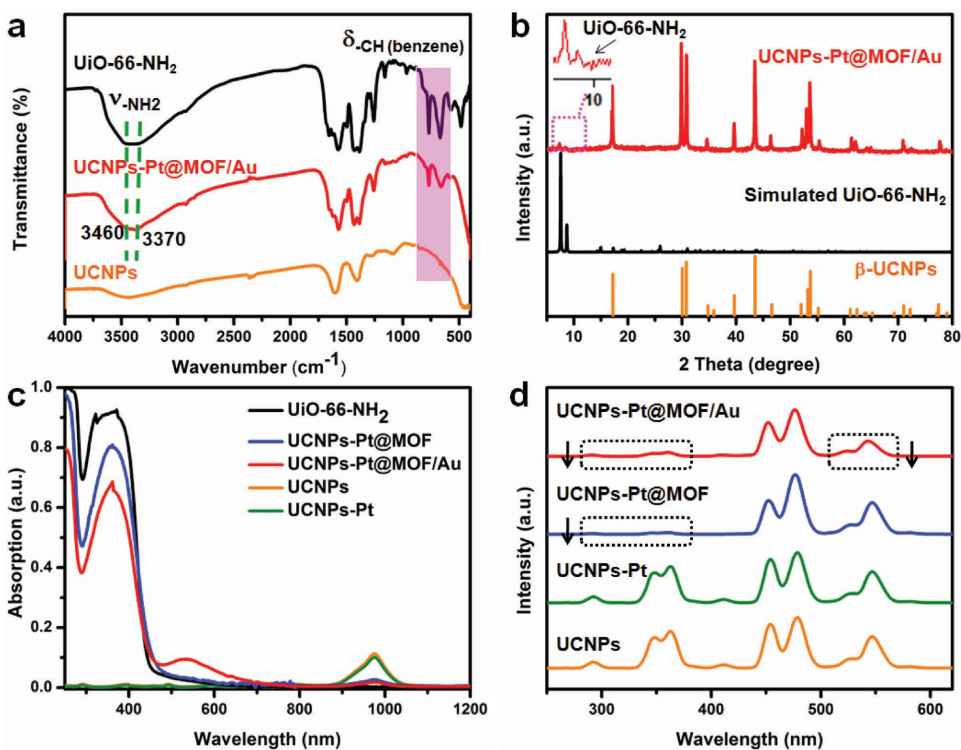


Figure 2. a) FT-IR spectra, (b) PXRD patterns, (c) UV-vis-NIR absorption spectra, and (d) upconversion luminescence spectra under excitation at 980 nm for different samples.

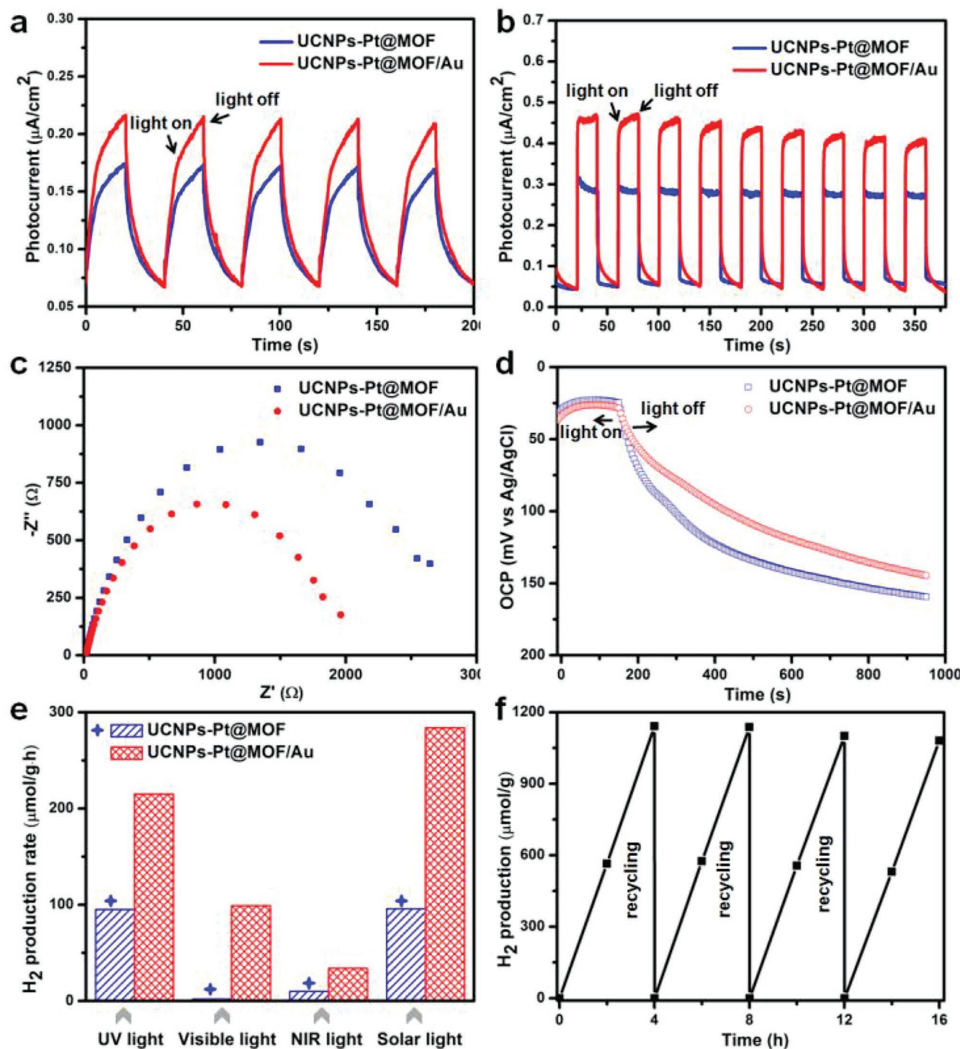


Figure 3. The photocurrent response of UCNP-Pt@MOF and UCNP-Pt@MOF/Au under (a) NIR light and (b) simulated solar light irradiation. c) EIS Nyquist plots, and (d) open-circuit potential as a function of time under NIR light irradiation for UCNP-Pt@MOF and UCNP-Pt@MOF/Au. e) Comparison of H₂ production rate of UCNP-Pt@MOF and UCNP-Pt@MOF/Au under UV (200–400 nm), visible (420–800 nm), NIR (980 nm), and simulated solar light irradiation. f) Recycling performance of UCNP-Pt@MOF/Au under simulated solar light.

absorption band in visible region from 500 to 600 nm appears, characteristic of the SPR of Au NPs. The combination of all these absorption features leads to the broadband photoresponse from UV to NIR region of UCNP-Pt@MOF/Au. The upconversion luminescence spectra have been further recorded (Figure 2d). Upon excitation by 980 nm laser light, both UCNP and UCNP-Pt give three peaks in UV region, two blue and two green emission peaks originated from the transitions of Tm³⁺ and Er³⁺ ions.^[8] Significantly, upon coating with UiO-66-NH₂, the UV emissions from UCNP almost quench due to the MOF absorption, given their good spectral overlap. Similarly, green emission (visible region) from UCNP is greatly weakened after the Au introduction, thanks to the SPR effect of Au NPs. These spectral changes unambiguously reflect the energy transfer between UCNP and MOF as well as Au NPs, resulting in the effective utilization of NIR light by MOF and Au NPs based on the inherent upconversion mechanism.

To ascertain the generation of electron–hole (e–h) pairs under light irradiation, photoelectrochemical experiments have been performed. There is a fast and uniform photocurrent response to each switch-on and -off event for UCNP-Pt@MOF and UCNP-Pt@MOF/Au under NIR irradiation (Figure 3a). The results clearly manifest that NIR light is able to induce e–h pairs, which is an essential step for subsequent photocatalysis. Moreover, the Au deposition further improves the e–h separation, as can be observed the higher photocurrent from UCNP-Pt@MOF/Au than UCNP-Pt@MOF under simulated solar light (Figure 3b). This argument is also supported by the electrochemical impedance spectroscopy (EIS) results (Figure 3c), in which UCNP-Pt@MOF/Au exhibits a smaller radius, indicative of a lower charge-transfer resistance. The results are in good agreement with open-circuit potential (OCP) response (Figure 3d), an indicator of electron transfer process on the catalyst surface, in which the decreased rate of OCP with light-off reflects the lifetime of charge carriers.^[9] The electric field

strength is weakened as the photo-induced electrons and holes move to opposite sides under NIR irradiation. However, when the light is off, this effect gradually disappears owing to the recombination of electrons and holes. Obviously, the slower decay of UCNPs-Pt@MOF/Au than UCNPs-Pt@MOF to flat potential implies the former a relatively long lifetime of charge carriers that is beneficial to photocatalysis.

Encouraged by the above characterization results, we set out to investigate photocatalytic H₂ production under UV (200–400 nm), visible (420–800 nm), and NIR (980 nm), as well as simulated solar light irradiations (Figure 3e). No obvious H₂ was produced with Au NPs or UCNPs as a catalyst regardless of irradiation wavelengths. All Pt-decorated composites exhibit exponentially enhanced activity in reference to UCNPs@MOF/Au and the parent MOF (Figure S5, Supporting Information), attributed to the greatly boosted e–h separation by the Pt electron sink, which is consistent with previous reports.^[7b,10] Furthermore, the H₂ production rate is improved with the Au-deposited composite, ≈2.26 times higher than that of UCNPs-Pt@MOF, under UV light irradiation. Due to the very weak absorption of UiO-66-NH₂ for visible light, the activity of the MOF and UCNPs-Pt@MOF is almost negligible under visible irradiation. Delightedly, the introduction of Au NPs makes the composite visible light-responsive and the H₂ production rate of UCNPs-Pt@MOF/Au reaches 99 μmol g⁻¹ h⁻¹ under visible irradiation. In addition, the wavelength dependent H₂ production rate of UCNPs-Pt@MOF/Au well coincides with the plasmon band of Au NPs (Figure S6, Supporting Information), clearly showing the contribution of Au SPR effect. Upon NIR excitation, the upconverted emissions in the UV and visible range can be absorbed by the MOF and Au NPs, respectively, based on energy transfer. Accordingly, H₂ can be produced by UCNPs-Pt@MOF and enhanced H₂ production activity can be observed for the Au loaded composite, UCNPs-Pt@MOF/Au. The NIR photoactivity (34 μmol g⁻¹ h⁻¹) is considerable, though it is lower than those under UV or visible irradiation, due to the well-known relatively low upconversion efficiency.^[5a] Noteworthy, the simultaneous harvesting of UV and visible light from UCNPs excited by NIR irradiation for photocatalytic H₂ production has never been reported yet. This work paves a way to the harnessing of NIR light for photocatalysis.

From the viewpoint of practical application, the photocatalytic activity under simulated solar light irradiation has been further examined. Significantly, the UCNPs-Pt@MOF/Au composite exhibits the highest H₂ production rate (280 μmol g⁻¹ h⁻¹), nearly three times that of UCNPs-Pt@MOF (96 μmol g⁻¹ h⁻¹). More importantly, the recycling experiments for UCNPs-Pt@MOF/Au demonstrate that no noticeable change occurs in the hydrogen production rate during the four catalytic cycles for 16 h (Figure 3f). TEM observation shows that the catalyst microstructure remains well after reaction (Figure S7, Supporting Information). PXRD patterns further support the structural integrity and crystallinity of the MOF shell and UCNPs (Figure S8, Supporting Information). On the basis of the above results, it is clear that the rationally designed UCNPs-Pt@MOF/Au composite is able to achieve full solar light-responsive photocatalytic H₂ production by taking advantages of plasmon and upconversion effects.

These catalytic results suggest that Au introduction is of great importance to the activity. Intuitively, it is necessary to adjust Au contents in the composites to optimize the H₂ production rate (Figure S5, Supporting Information). Regardless of the light in UV, visible or NIR region, the increased Au contents results in a higher H₂ production rate in UCNPs-Pt@MOF/Au composites; when the Au loading is higher than 0.3 wt%, the photocatalytic activity starts to decrease, suggesting that all above activities obtained for UCNPs-Pt@MOF/Au with 0.3 wt% Au content are optimized. Too high Au loadings might create structural defects at the MOF/Au interface, leading to new recombination centers to accelerate e–h recombination and/or the light shielding effect by Au NPs.^[11]

Based on the above experimental results, the enhanced photocatalytic activity of UCNPs-Pt@MOF/Au under UV, visible, and NIR light irradiation should be ascribed to different mechanisms (Figure 4a–c). Exposure to UV light, the MOF is excited and the electrons would be transferred to Pt, which behave as electron reservoirs and active sites for subsequent proton reduction (Figure 4a). Electron spin resonance (ESR) measurements reveal the generation of Zr^{III} intermediate or oxygen vacancy in Zr-oxo clusters via electron transfer for both UCNPs-Pt@MOF (Figure 4d) and UCNPs-Pt@MOF/Au (Figure 4e).^[7b,11b,12] With the help of Au SPR effect, the composite clearly displays significant visible-light photoactivity. The SPR-excited hot electrons of Au are injected to the lowest unoccupied molecular orbital (LUMO) of the MOF, then rapidly transfer to Pt sites to generate H₂ (Figure 4b). This is supported by ESR measurements, in contrast to the evidently enhanced signal ($g = 2.003$) for UCNPs-Pt@MOF/Au, UCNPs-Pt@MOF gave maintained signal under visible irradiation (green and pink marks in Figure 4d,e). Things become more complicated under NIR irradiation (Figure 4c). Upon being excited by NIR light, Tm³⁺ and Er³⁺ ions in UCNPs are excited due to efficient energy transfer from Yb³⁺ to them. The upconverted UV emission from Tm³⁺ can be absorbed by the MOF to generate e–h pairs, identical to be excited by the direct UV irradiation. The excited electrons are transferred to Pt sites for proton reduction. It is noteworthy that, H₂ generation on Au particles would be negligible as compared to that on Pt particles, as evidenced by the significantly higher H₂ production rate of UCNPs-Pt@MOF than UCNPs@MOF/Au (Figure S9, Supporting Information). Simultaneously, the upconverted green emission from Er³⁺ is harvested by Au NPs, thanks to their SPR effect, followed by a similar electron transfer pathway to that for UCNPs-Pt@MOF/Au under visible irradiation. Charge separation takes place in Au NPs by transferring hot electrons to MOF. As a result, both energy transfer processes from UCNPs to the MOF and Au NPs greatly improve the NIR-light and thus simulated solar light photocatalytic activity.

In summary, the UCNPs-Pt@MOF/Au composites featuring broadband light absorption from UV to NIR region has been rationally designed and fabricated, taking advantages of plasmon and upconversion effects. Thanks to the response to broad spectral solar light, the composites exhibit considerable photocatalytic H₂ production activities under UV, visible or even NIR irradiation, which represents the first work reporting H₂ production photocatalysts with considerable activity toward all these three regions of light irradiation. Remarkably, the structure of the composites can be well tailored including the MOF

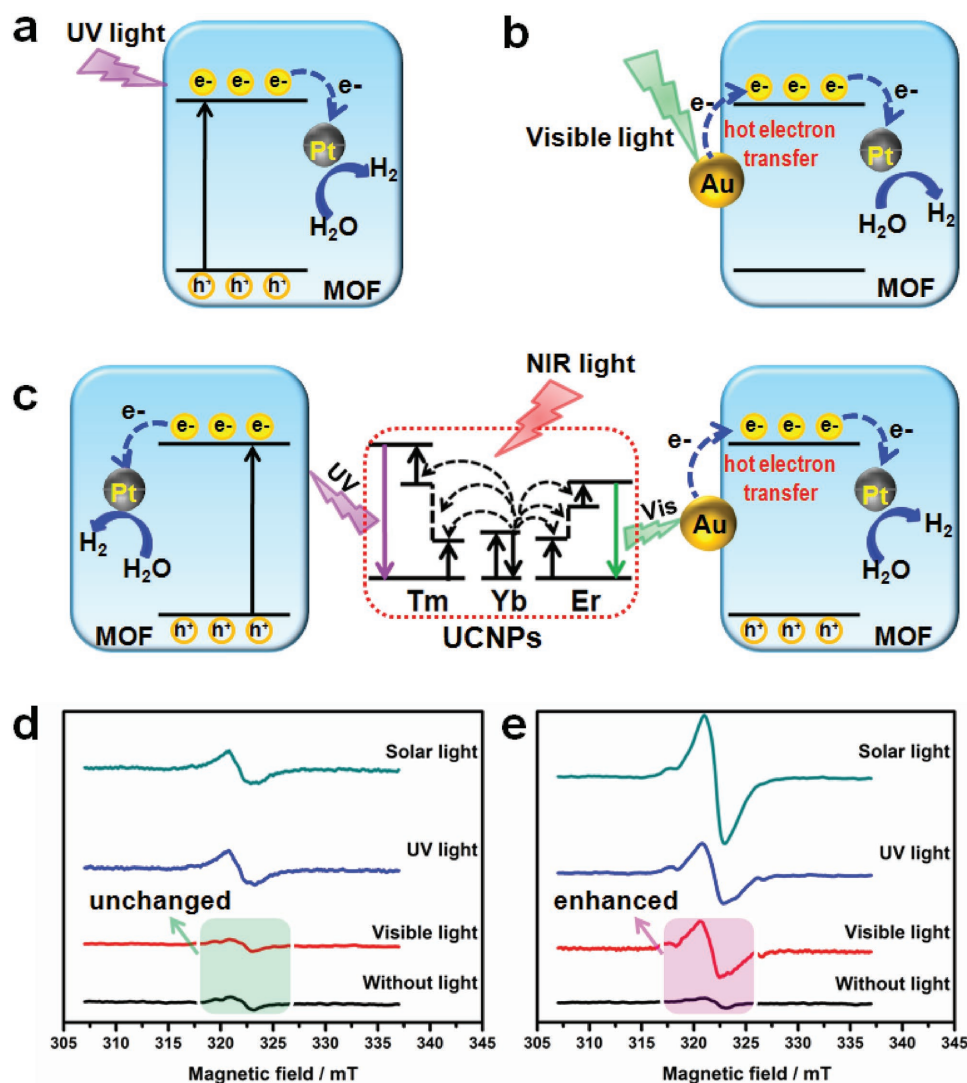


Figure 4. Schematic illustration of H₂ production mechanisms for UCNPs-Pt@MOF/Au under (a) UV, (b) visible, and (c) NIR light irradiation, respectively. ESR spectra of (d) UCNPs-Pt@MOF and (e) UCNPs-Pt@MOF/Au in dark or under light irradiation for 120 s, the green and the pink markers highlight the unchanged and enhanced signal changes, respectively.

thickness and Au contents, and the optimized composite offers not only promising H₂ production rate as high as 280 $\mu\text{mol g}^{-1} \text{h}^{-1}$ but also excellent recycling performance under simulated solar light irradiation. The involved photocatalytic mechanisms under light irradiation falling in different wavelength ranges have been elucidated. This first integration of plasmon and upconversion effects into MOF composites greatly extends light absorption, and Pt further boosts the charge separation, realizing the excellent photocatalysis toward all three regions in full solar light. This work opens up a new avenue to the development of novel and efficient composite photocatalysts harvesting solar spectrum as broad as possible.

Supporting Information

Supporting Information is available from the Wiley Online Library or from the author.

Acknowledgements

This work was supported by the National Natural Science Foundation of China (21725101, 21673213, 21701160, and 21521001), the National Research Fund for Fundamental Key Project (2014CB931803), the General Financial Grant from the China Postdoctoral Science Foundation (2016M602018), and the Recruitment Program of Global Youth Experts.

Conflict of Interest

The authors declare no conflict of interest.

Keywords

full solar light, metal–organic frameworks, near-infrared light, photocatalysis, photocatalytic H₂ production

Received: December 18, 2017
Revised: March 4, 2018
Published online: May 15, 2018

- [1] a) A. Fujishima, K. Honda, *Nature* **1972**, 238, 37; b) S. N. Habisreutinger, L. Schmidt-Mende, J. K. Stolarczyk, *Angew. Chem., Int. Ed.* **2013**, 52, 7372; c) A. Dhakshinamoorthy, A. M. Asiri, H. Garcia, *Angew. Chem., Int. Ed.* **2016**, 55, 5414; d) T. Hisatomi, J. Kubota, K. Domen, *Chem. Soc. Rev.* **2014**, 43, 7520; e) X. Chen, S. Shen, L. Guo, S. S. Mao, *Chem. Rev.* **2010**, 110, 6503; f) Q. Lin, X. Bu, C. Mao, X. Zhao, K. Sasan, P. Feng, *J. Am. Chem. Soc.* **2015**, 137, 6184; g) J. R. Ran, B. C. Zhu, S. Z. Qiao, *Angew. Chem., Int. Ed.* **2017**, 56, 10373; h) L. Chen, K. Furukawa, J. Gao, A. Nagai, T. Nakamura, Y. Dong, D. Jiang, *J. Am. Chem. Soc.* **2014**, 136, 9806.
- [2] a) H. Li, X. He, Z. Kang, H. Huang, Y. Liu, J. Liu, S. Lian, C. H. A. Tsang, X. Yang, S.-T. Lee, *Angew. Chem., Int. Ed.* **2010**, 49, 4430; b) Y. Sang, H. Liu, A. Umar, *ChemCatChem* **2015**, 7, 559; c) G. Wang, B. Huang, X. Ma, Z. Wang, X. Qin, X. Zhang, Y. Dai, M.-H. Whangbo, *Angew. Chem., Int. Ed.* **2013**, 52, 4810; d) X. Li, Z. Li, J. Yang, *Phys. Rev. Lett.* **2014**, 112, 018301; e) X. Xia, N. Deng, G. Cui, J. Xie, X. Shi, Y. Zhao, Q. Wang, W. Wang, B. Tang, *Chem. Commun.* **2015**, 51, 10899.
- [3] a) R. Asahi, T. Morikawa, T. Ohwaki, K. Aoki, Y. Taga, *Science* **2001**, 293, 269; b) Z. Zou, J. Ye, K. Sayama, H. Arakawa, *Nature* **2001**, 414, 625; c) E. Reisner, D. J. Powell, C. Cavazza, J. C. Fontecilla-Camps, F. A. Armstrong, *J. Am. Chem. Soc.* **2009**, 131, 18457; d) F.-K. Meng, Z.-L. Hong, J. Arndt, M. Li, M.-J. Zhi, F. Yang, N.-Q. Wu, *Nano Res.* **2012**, 5, 213; e) D. M. Schultz, T. P. Yoon, *Science* **2014**, 343, 1239176; f) X. Wang, F. Wang, Y. Sang, H. Liu, *Adv. Energy Mater.* **2017**, 7, 1700473.
- [4] a) S. Linic, P. Christopher, D. B. Ingram, *Nat. Mater.* **2011**, 10, 911; b) W. B. Hou, S. B. Cronin, *Adv. Funct. Mater.* **2013**, 23, 1612; c) Q. Xiao, E. Jaatinen, H. Zhu, *Chem. Asian J.* **2014**, 9, 3046; d) Z.-Z. Lou, Z.-Y. Wang, B.-B. Huang, Y. Dai, *ChemCatChem* **2014**, 6, 2456; e) L. Liu, S. Ouyang, J. Ye, *Angew. Chem., Int. Ed.* **2013**, 52, 6689; f) N. N. Jiang, X. L. Zhuo, J. F. Wang, *Chem. Rev.* **2018**, 118, 3054.
- [5] a) F. Wang, X. Liu, *Chem. Soc. Rev.* **2009**, 38, 976; b) Y. Li, J. Tang, L. He, Y. Liu, Y. Liu, C. Chen, Z. Tang, *Adv. Mater.* **2015**, 27, 4075; c) Y. Tang, W. Di, X. Zhai, R. Yang, W. Qin, *ACS Catal.* **2013**, 3, 405; d) Z. Xu, M. Quintanilla, F. Vetrone, A. O. Govorov, M. Chaker, D. Ma, *Adv. Funct. Mater.* **2015**, 25, 2950; e) M. Li, Z. Zheng, Y. Zheng, C. Cui, C. Li, Z. Li, *ACS Appl. Mater. Interfaces* **2017**, 9, 2899.
- [6] a) H.-C. Zhou, J. R. Long, O. M. Yaghi, *Chem. Rev.* **2012**, 112, 673; b) H.-C. Zhou, S. Kitagawa, *Chem. Soc. Rev.* **2014**, 43, 5415; c) H. Furukawa, K. E. Cordova, M. O'Keeffe, O. M. Yaghi, *Science* **2013**, 341, 1230444; d) T. R. Cook, Y.-R. Zheng, P. J. Stang, *Chem. Rev.* **2013**, 113, 734; e) M. Kandiah, M. H. Nilsen, S. Usseglio, S. Jakobsen, U. Olsbye, M. Tilset, C. Larabi, E. A. Quadrelli, F. Bonino, K. P. Lillerud, *Chem. Mater.* **2010**, 22, 6632; f) C. Gomes Silva, I. Luz, F. X. Llabrés i Xamena, A. Corma, H. García, *Chem.-Eur. J.* **2010**, 16, 11133; g) T. Islamoglu, S. Goswami, Z. Li, A. J. Howarth, O. K. Farha, J. T. Hupp, *Acc. Chem. Res.* **2017**, 50, 805; h) B. Li, H.-M. Wen, Y. Cui, W. Zhou, G. Qian, B. Chen, *Adv. Mater.* **2016**, 28, 8819.
- [7] a) M. Zhao, K. Yuan, Y. Wang, G. Li, J. Guo, L. Gu, W. Hu, H. Zhao, Z. Tang, *Nature* **2016**, 539, 76; b) J.-D. Xiao, Q. Shang, Y. Xiong, Q. Zhang, Y. Luo, S.-H. Yu, H.-L. Jiang, *Angew. Chem., Int. Ed.* **2016**, 55, 9389; c) Q. Yang, Q. Xu, H.-L. Jiang, *Chem. Soc. Rev.* **2017**, 46, 4774; d) T. Zhang, W. Lin, *Chem. Soc. Rev.* **2014**, 43, 5982; e) Y. Fu, D. Sun, Y. Chen, R. Huang, Z. Ding, X. Fu, Z. Li, *Angew. Chem., Int. Ed.* **2012**, 51, 3364; f) T. Zhou, Y. Du, A. Borgna, J. Hong, Y. Wang, J. Han, W. Zhang, R. Xu, *Energy Environ. Sci.* **2013**, 6, 3222; g) S. Pullen, H. Fei, A. Orthaber, S. M. Cohen, S. Ott, *J. Am. Chem. Soc.* **2013**, 135, 16997; h) Z.-L. Wu, C.-H. Wang, B. Zhao, J. Dong, F. Lu, W.-H. Wang, W.-C. Wang, G.-J. Wu, J.-Z. Cui, P. Cheng, *Angew. Chem., Int. Ed.* **2016**, 55, 4938; i) S. Yang, B. Pattengale, E. L. Kovrigin, J. Huang, *ACS Energy Lett.* **2017**, 2, 75; j) Y. Zhang, J. Guo, L. Shi, Y. Zhu, K. Hou, Y. Zheng, Z. Tang, *Sci. Adv.* **2017**, 3, e1701162; k) X.-Y. Dong, M. Zhang, R.-B. Pei, Q. Wang, D.-H. Wei, S.-Q. Zang, Y.-T. Fan, T. C. W. Mak, *Angew. Chem., Int. Ed.* **2016**, 55, 2073; l) J.-D. Xiao, L. Han, J. Luo, S.-H. Yu, H.-L. Jiang, *Angew. Chem., Int. Ed.* **2018**, 57, 1103; m) X. Fang, Q. Shang, Y. Wang, L. Jiao, T. Yao, Y. Li, Q. Zhang, Y. Luo, H.-L. Jiang, *Adv. Mater.* **2018**, 30, 1705112.
- [8] J. Zhou, Q. Liu, W. Feng, Y. Sun, F. Li, *Chem. Rev.* **2015**, 115, 395.
- [9] a) J. Kim, W. Choi, *Energy Environ. Sci.* **2010**, 3, 1042; b) Y. Sang, Z. Zhao, M. Zhao, P. Hao, Y. Leng, H. Liu, *Adv. Mater.* **2015**, 27, 363.
- [10] a) C. Wang, K. E. DeKrafft, W. Lin, *J. Am. Chem. Soc.* **2012**, 134, 7211; b) S. Wang, X. Wang, *Small* **2015**, 11, 3097.
- [11] a) Q. Zhang, D. Q. Lima, I. Lee, F. Zaera, M. Chi, Y. Yin, *Angew. Chem., Int. Ed.* **2011**, 50, 7088; b) H. Li, F. Qin, Z. Yang, X. Cui, J. Wang, L. Zhang, *J. Am. Chem. Soc.* **2017**, 139, 3513.
- [12] a) D. Sun, Y. Fu, W. Liu, L. Ye, D. Wang, L. Yang, X. Fu, Z. Li, *Chem. Eur. J.* **2013**, 19, 14279; b) H.-Q. Xu, J. Hu, D. Wang, Z. Li, Q. Zhang, Y. Luo, S.-H. Yu, H.-L. Jiang, *J. Am. Chem. Soc.* **2015**, 137, 13440.